PERGAMON

International Journal of Heat and Mass Transfer 45 (2002) 3947–3959

International Journal of HEAT and MASS TRANSFER

www.elsevier.com/locate/ijhmt

Interfacial heat transfer during subcooled flow boiling

Gopinath R. Warrier, Nilanjana Basu, Vijay K. Dhir *

Department of Mechanical and Aerospace Engineering, University of California, 420 Westwood Plaza, Los Angeles, CA 90095, USA

Received 2 November 2001; received in revised form 2 March 2002

Abstract

In order to develop a mechanistic model for the subcooled flow boiling process, the key issues which must be addressed are wall heat flux partitioning and interfacial (condensation) heat transfer. The sink term in the two-fluid models for void fraction prediction is provided by the condensation rate at the vapor–liquid interface. Low pressure subcooled flow boiling experiments, using water, were performed using a vertical flat plate heater to investigate the bubble collapse process. A high-speed CCD camera was used to record the bubble collapse in the bulk subcooled liquid. Based on the analyses of these digitized images, bubble collapse rates and the associated heat transfer rate were determined. The experimental data were in turn used to correlate the bubble collapse rate and the interfacial heat transfer rate. These correlations are functions of bubble Reynolds number, liquid Prandtl number, Jacob number, and Fourier number. The correlations account for both the effect of forced convection heat transfer and thickening of the thermal boundary layer as the vapor bubble condenses which in turn makes the condensation heat transfer time dependent. Comparison of the measured experimental data with those predicted from the correlations show that predictions are well within ±25% of the experimentally measured values. These correlations have also been compared with those available in the literature.

Keywords: Bubble condensation; Subcooled boiling

1. Introduction

In order to develop a mechanistic model for the subcooled flow boiling process, the key issues which must be addressed are wall heat flux partitioning and interfacial (condensation) heat transfer. Mechanistic models involve modeling each of the individual physical mechanisms associated with the process which when combined can be used to develop larger global models. Since the source and sink terms in the two-fluid models, such as RELAP5 [1], used to predict axial void fraction variation during subcooled boiling are provided by the rate at which vapor is added to the bulk and the condensation rate at the vapor–liquid interface, respectively, any error in the calculation of these quantities will introduce large errors in the calculation of the void fraction. An extensive review of the available literature (Warrier and Dhir [2]) has revealed that very limited data are available to develop and validate a mechanistic model for subcooled flow boiling. Hence, the present investigation was undertaken to address the issue of the interfacial heat transfer. This paper deals with experiments performed to measure the condensation heat transfer rate from vapor bubbles during subcooled flow boiling of water at low pressures.

A number of studies have been performed previously to study condensing bubbles in a subcooled liquid. Some of the notable studies are those by Isenberg and Sideman [3], Chen and Mayinger [4], and Zeitoun et al. [5]. All of these investigations were aimed at developing correlations/models for bubble diameter $\beta = D_b/D_{bo}$, where D_b is the instantaneous bubble diameter and D_{bo} is the initial bubble diameter (which is the bubble lift-off diameter) as a function of time and the corresponding heat transfer coefficient ($Nu_c = h_c D_b/k_l$) associated with the condensing bubble. Isenberg and Sideman [3] studied bubble condensation in immiscible liquids. Single

* Corresponding author. Tel.: +1-310-825-9617; fax: +1-310-206-4830.

E-mail address: vdhir@seas.ucla.edu (V.K. Dhir).

0017-9310/02/$ - see front matter
PII: S0017-9310(02)00102-3

Nomenclature

A	area
C_p	specific heat
D	diameter
Fo	Fourier number
G	mass flux
h	heat transfer coefficient
h_{fg}	latent heat
Ja	Jacob number
k	thermal conductivity
Nu	Nusselt number
P	pressure
Pr	Prandtl number
q	heat flux
Re	bubble Reynolds number
t	time
T	temperature
ΔT	temperature difference
U	velocity
V	volume
x	cartesian coordinate
y	cartesian coordinate
z	cartesian coordinate

Greek symbols

α	void fraction or thermal diffusivity
β	dimensionless bubble diameter
ϕ	contact angle
μ	kinematic viscosity
ρ	density

Subscripts

b	bubble
bs	bubble (based on Sauter diameter)
c	condensation
i	interface
l	liquid
o	initial condition
rel	relative
sat	saturation
sub	subcooled
v	vapor
w	wall

bubbles of volatile organic fluids (pentane or *iso*-pentane) cooling under heat transfer controlled conditions while rising freely in water and aqueous glycerol solution were studied by them, both theoretically and experimentally. Their theoretical analysis was based on the assumption that the flow around the collapsing sphere was a potential flow. The bubble collapse rate correlation developed by them agreed well with their experimental data for bubble sizes in the range 3 mm $< D_{bo} <$ 10 mm.

Chen and Mayinger [4] used holographic interferometry and high-speed cinematography to study the heat transfer at the interface of vapor bubbles condensing in a subcooled liquid, for both attached bubbles as well as departing bubbles. Their experiments, performed using ethanol, propanol, R113, and water as the working fluids, covered the following range of parameters: $2 < Pr_l < 15$ and $1 < Ja < 120$, where the Prandtl number (Pr_l) and Jacob number (Ja) are defined as $Pr_l = \mu_l C_{p,l}/k_l$ and $Ja = \rho_l C_{p,l}\Delta T_{sub}/\rho_v h_{fg}$, $\Delta T_{sub} = T_{sat} - T_l$. In these experiments, the vapor bubbles were generated using a nozzle of diameter 1.6 mm. They developed correlations to predict both β and Nu_c as functions of time.

Zeitoun et al. [5] performed experiments in subcooled water-steam bubbly flow in a vertical conduit. The bubble condensation process, recorded using a high-speed camera, was used to obtain bubble diameter and condensation heat transfer data. They developed correlations for β and Nu_c. However, unlike previous correlations, their Nu_c correlation involved the void fraction (α) and is based on the mean Sauter diameter ($D_{bs} = 6V_b/A_b$, where V_b and A_b are the bubble volume and surface area, respectively) of the bubble. In developing the correlation for β, by integrating the Nu_c correlation, D_{bs} was assumed to represent the instantaneous bubble diameter. The void fraction was included to account for the presence of multiple bubbles. Their correlation is valid for void fraction in the range of $0.02 < \alpha < 0.3$ and for bubble relative velocities ($U_{b,rel}$) in the range of $0.2 < U_{b,rel} < 0.4$ m/s. The major difficulty in applying their correlation is the fact that α needs to be known and that it is not a transient model. A listing of the correlations discussed above is given in Table 1.

Although a number of correlations have been reported in the literature for condensation of bubbles translating in a subcooled liquid (see Zeitoun et al. [5] for details), most of these correlations are based on theoretical and experimental studies performed where only bubbles rising in a stagnant liquid were considered. Also, as pointed out by Zeitoun et al. [5], there is considerable discrepancy in these correlations as regards to the effect of Ja on Nu_c. The experimental database currently available for steam bubbles collapsing in flowing water is very limited. This particular flow situation is of interest due to it direct application to nuclear reactor systems. Thus, the goal of this study was to investigate the interfacial heat transfer that occurs during subcooled

Table 1
List of dimensionless bubble diameter and condensation Nusselt number correlations

Authors	Bubble collapse (β) and condensation Nusselt numbers (Nu_c) correlations
Isenberg and Sideman [3]	$\beta = (1 - 3/\pi^{1/2} Ja\, Re_{bo}^{1/2} Pr_l^{1/3} Fo_o)^{2/3}$, $Nu_c = 1/\pi^{1/2} Re_b^{1/2} Pr_l^{1/3}$
Chen and Mayinger [4]	$\beta = (1 - 0.56 Re_{bo}^{0.7} Pr_l^{0.5} Ja\, Fo_o)^{0.9}$, $Nu_c = 0.185 Re_b^{0.7} Pr_l^{1/2}$
Zeitoun et al. [5]	$\beta = (1 - 5.67 Re_{bo}^{0.61} \alpha^{0.328} Ja^{0.629} Fo_o)^{0.72}$, $Nu_c = 2.04 Re_b^{0.61} \alpha^{0.328} Ja^{-0.308}$

flow boiling of water. The experimental data gathered during this study was used to expand the experimental database and develop relevant correlations.

2. Experimental apparatus

The schematic of the flow loop is shown in Fig. 1. The flow loop consists of two tanks, each with a volume of 1.25 m^3, a centrifugal pump, turbine flow meter, bypass line, preheater, and test section. Tank #1, which was used as the supply tank, is also fitted with immersion heaters (13.5 kW total power) to degas and preheat the distilled water used in the experiments. The preheater consisted of a 210 kW (480 V, 3 phase) flanged immersion heater fitted vertically onto a stainless steel container. The power to the immersion heater is controlled using a 480 V, 350 A silicon controlled rectifier (SCR) power controller (Phasetronics). Using the power controller and thermocouple outputs, it is possible to control the liquid subcooling accurately. The flow channel is 1.83 m long, of which the heated section length is 0.30 m. A 0.61 m long flow development section is provided upstream of the heated section, while a 0.30 m long section is provided downstream of the heated section. In addition, transition sections, each 0.30 m long, are provided upstream and downstream of the test section. A flow straightener is also provided at the inlet of the flow developing section. The cross-section of the flow channel is shown in Fig. 2. The flow channel is almost square in cross-section with a flow area of 16.33 cm^2. The copper block, which is heated, is mounted flush with one of the inside walls of the flow channel, while pyrex glass windows are provided on the other three sides of the channel. The glass windows help in visual observation of the flow. Rubber gaskets provided at all the joints ensure that there are no leaks.

Fig. 3 shows the dimensions of the copper heating block and the placement of the thermocouples at each axial location. The temperatures measured by these embedded thermocouples are used to determine the temperature and heat flux at the surface (boiling surface). The thermocouples (K-type, 3.17 mm diameter) are located at seven different axial locations along the length of the copper block. At each axial location, there are nine thermocouples (labelled 1 through 9) embedded in the block at discrete locations normal to the heating surface, as can be seen from the cross-section of the copper block shown in Fig. 3. Thus, a total of 63 thermocouples are provided in the copper block. Each of these thermocouples was silver soldered in place in order to ensure accurate temperature measurements. The heating of the copper block is achieved using 36 cartridge heaters embedded in the back of the copper block. These cartridge heaters were arranged such that the heat flux at the boiling surface is uniform. Since each cartridge heater has a maximum power rating of 750 W, the total

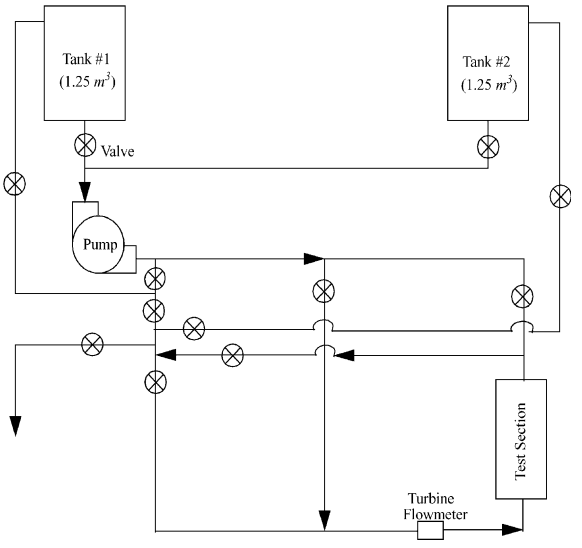

Fig. 1. Schematic of test loop.

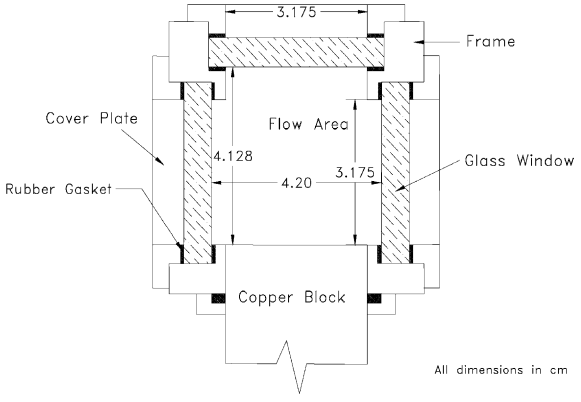

Fig. 2. Cross-section of test chamber.

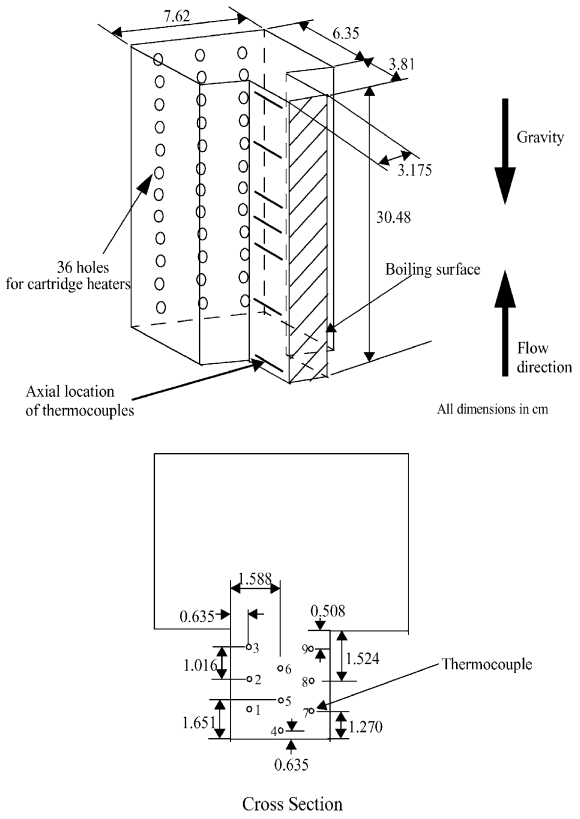

Fig. 3. Copper heating block and thermocouple placement.

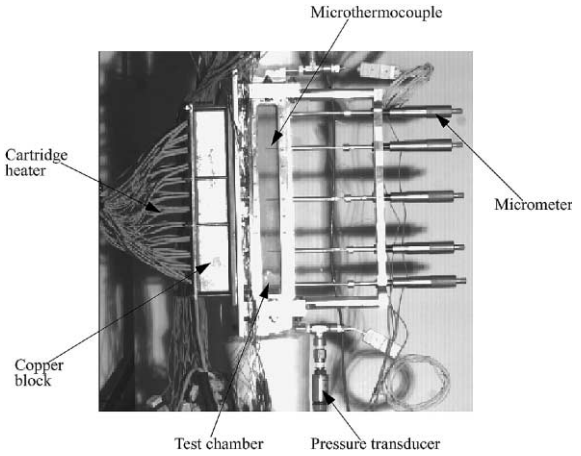

Fig. 4. Photograph of test chamber.

installed power in the test section is 27 kW. The power supplied to the cartridge heaters, and hence to the copper block, is controlled with a 240 V, 50 A SCR power controller (Phasetronics). Additional details regarding the test section can be found in the report by Warrier et al. [6].

Fig. 4 shows a photograph of the assembled test section with the various pressure and temperature sensors mounted. Five microthermocouples (K-type, 0.25 mm diameter) are mounted in the test chamber to measure the liquid temperature profile. These microthermocouples are connected to micrometers (0.025 mm resolution) making it possible to traverse the width of the channel. They measure liquid temperatures at axial distances 0.64, 6.48, 15.25, 24.00, and 29.86 cm from the leading edge of the copper block. Additional thermocouples and pressure transducers are installed at the inlet and exit of the heating section. The thermocouples (K-type, 0.81 mm diameter) are used to measure the mean fluid temperatures, while the pressure transducers (Omega, Model PX202-100GV) are used to measure the system pressures at the inlet and exit, respectively.

Before each experiment, tank #1 was filled with distilled water and is heated. The water was degassed by boiling it for approximately three hours and then cooling to the required temperature. During an experiment, water was pumped from tank #1, passed through the flowmeter, inline preheater, and the test section before being discharged into tank #2. The liquid flow rate was controlled using the valve at the preheater inlet and the bypass line. The power to the boiling surface was turned on once the required flow rate and liquid subcooling levels at inlet were achieved. Once the test heater reached steady state, all the required temperature measurements were recorded. A 16-bit data acquisition system (Strawberry Tree, Model DS-16-8-TC) was used to record the temperatures. The boiling phenomena occurring at the heater surface was recorded using a high-speed CCD camera (HISIS 2000, KSV Instruments Ltd.). This camera is capable of recording pictures with a resolution of 256×256 pixels and has a maximum frame rate of 1220 frames/s. This camera is capable of being fitted with lenses of various focal lengths as per experimental requirements.

This section discusses the uncertainty of the measured experimental data. The uncertainty in the thermal conductivity (k) of the copper block is estimated to be approximately 1%. The uncertainty in the temperature measurements inside the copper block is ± 0.2 °C, while the uncertainty in the placement of the thermocouples is estimated to be ± 0.5 mm. Based on these uncertainties, the error in the calculated wall heat fluxes of 20, 53, and 96 W/cm^2 are $\pm 9.4\%$, $\pm 8.9\%$, and $\pm 8.7\%$, respectively. As mentioned earlier, the surface temperature of the heater was determined by extrapolating the interior temperature to the surface. The uncertainty in these calculated heater surface temperatures is in the range ± 0.4 to ± 0.8 °C. The error associated with the measured liquid temperature is ± 0.2 °C and that in the probe position is ± 0.025 mm.

The error in the measurement of the bubble diameters is ±0.02 mm, which is largely due to the resolution of the recorded images. As a result, the maximum uncertainty in β is about ±9%. The error in the measurement of the bubble position is ±0.02 mm. The estimated maximum uncertainty in the bubble relative velocity is ±14%. The uncertainty in the measurement of the liquid subcooling is ±0.4 °C. Based on the above measurement uncertainties, the maximum error in the values of Nu_c is estimated to be ±28%.

3. Experimental results and data reduction

A total of 24 subcooled boiling experiments were performed as part of this study. The flow conditions for which these experiments were performed are listed in Table 2. The contact angles (ϕ) measured at the start of each experiment are also given in Table 2. The contact angle is defined as the angle between the tangent to the bubble and the solid surface, measured from the liquid side. Details of how the boiling surface was prepared and the contact angle measured can be found in Warrier et al. [6].

In each run, the wall heat flux was computed from the measured temperature gradient in the copper block. The total power supplied was also measured. A comparison of the measured and calculated total power shows that the difference is approximately 1.7% which suggests that the heat loss from the copper block for this case was less than 1.7% on an average for all cases.

The heater surface temperatures were determined by extrapolating the measured interior temperatures to the surface. The liquid temperature profile was measured at five axial locations using traversable microthermocouples. The typical response time of these microthermocouples is about 5–7 ms. Though it is possible to distinguish between the liquid and vapor phases, since the temperature data was only sampled at a rate of 1.0–3.0 Hz, the response of the microthermocouples could not be used to measure the instantaneous liquid and vapor phases. The average liquid temperature was then determined by averaging the lowest temperatures measured for each particular temperature series recorded. Fig. 5 shows the typical liquid temperatures at various axial locations as a function of the normal distance (y) to the heater surface. It must be mentioned that the liquid temperature data shown in Fig. 5 is time-averaged value (over a time period of 30 s). From Fig. 5, it is clear that a large temperature gradient exists close to the heated wall, while far from the wall the liquid temperature is the bulk liquid temperature. In Fig. 5, the

Table 2
Operating conditions for subcooled boiling experiments

No.	Mass flux (G, kg/m^{2}s)	Pressure (P, bar)	Inlet liquid subcooling (ΔT_{sub}, °C)	Heat flux (q_w, W/cm^2)	Contact angle (ϕ, deg)
TP1	340	1.03	14.5	20.6	29.6
TP2	340	1.03	46.5	41.7	28.3
TP3	340	1.03	35.0	36.3	29.6
TP4	235	1.03	41.0	21.0	30.0
TP5	684	1.03	34.0	35.8	30.6
TP6	340	1.03	24.0	40.7	31.3
TP7	348	1.03	22.8	20.0	31.3
TP7a	348	1.03	23.6	34.5	31.3
TP7b	348	1.03	23.0	16.0	31.3
TP8	348	1.03	38.5	45.4	30.0
TP8a	348	1.03	37.2	29.0	30.0
TP9	346	1.03	11.1	41.6	29.4
TP9a	346	1.03	9.0	18.0	29.4
TP9b	346	1.03	10.3	9.9	29.4
TP10a	342	1.03	7.0	9.6	30.5
TP10b	342	1.03	8.0	21.9	30.5
TP10c	342	1.03	7.7	40.2	30.5
TP11a	346	1.03	10.8	53.6	29.2
TP11b	346	1.03	11.1	69.8	29.2
TP11c	346	1.03	11.1	96.3	29.2
TP12a	346	1.03	12.9	16.0	90.0
TP12c	346	1.03	10.2	49.0	90.0
TP12d	350	1.03	11.6	64.3	90.0
TP12e	350	1.03	10.7	94.4	90.0

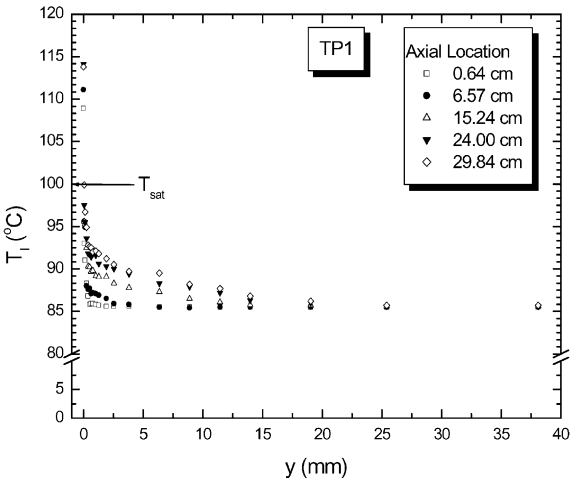

Fig. 5. Liquid temperature profile for test case TP1.

temperature gradients close to the wall are 311.7, 303.9, 321.6, 325.5, and 273.6 °C/mm at axial locations 0.64, 6.57, 12.24, 24.00, and 29.84 cm, respectively. Due to the large temperature gradient close to the wall, any small error in computing the gradient can result in large errors in the computed heat flux. Referring to Fig. 5, though the extrapolated heater surface temperature (114.1 °C) at axial location 24.00 cm is higher than that at axial location 29.84 cm (113.8 °C) it is within the uncertainty limits.

The condensation heat transfer coefficient for detached bubbles was calculated by measuring the bubble diameter as a function of time. The bubble pictures were taken with the camera placed on one side of the test chamber with the light source (with filter) placed on the opposite side. By analyzing the movies recorded using the CCD camera, frame by frame using a frame grabber, the diameter of the bubble and its position (both in the axial direction and in the direction normal to the heating surface) as a function of time was determined. All movies in this study were recorded using a frame rate of 1220 frames/s. During the recording stage, care was taken not to change the focus of the camera. After the bubble pictures were taken, a reference scale was placed

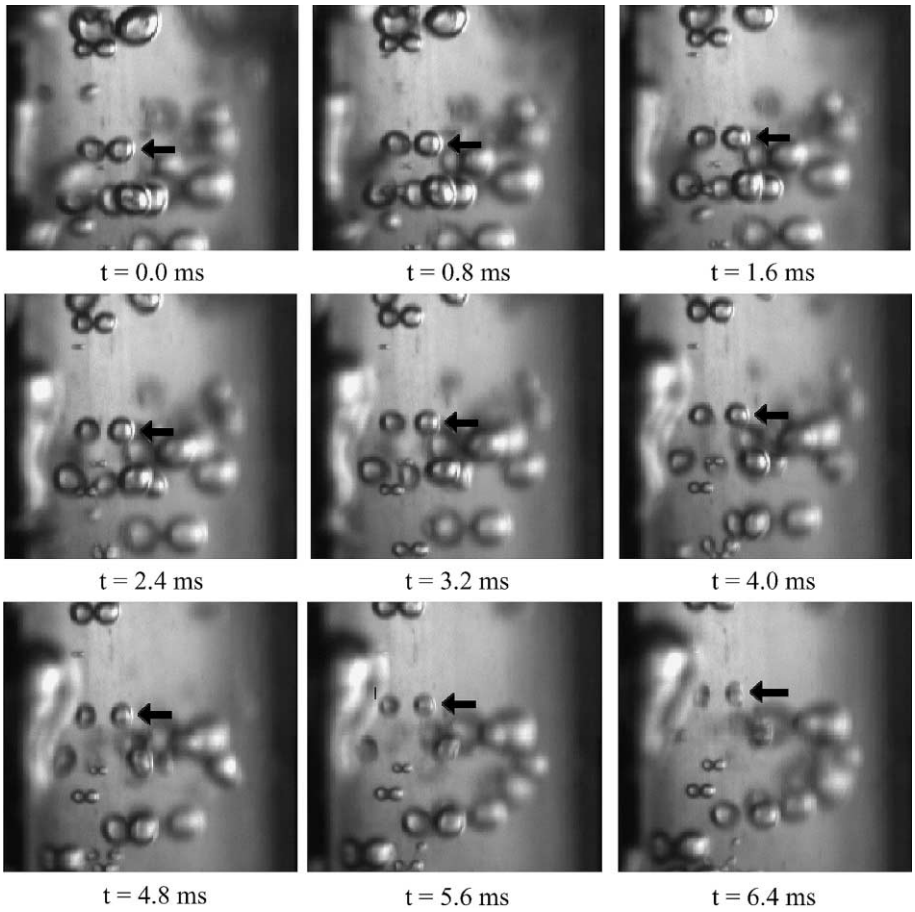

Fig. 6. Photographs showing bubble collapse sequence.

on the outside of the test chamber and the camera was moved back (without adjusting the focus of the camera) such that the reference scale was in focus. A picture of the reference scale was then taken and subsequently used to scale the bubble diameters. In analyzing these movie frames, only those bubbles that could be observed lifting off the heater surface and moving into the bulk liquid were considered. The bubble diameters calculated in this study were in fact the volume equivalent bubble diameters, which were calculated as follows: for each bubble of interest, assuming the bubble to be an ellipsoid, the major and minor diameters were measured. Then the bubble volume was determined assuming the bubble to be a body of revolution. Now considering the bubble to be a sphere of the same volume, the volume equivalent bubble diameter was determined. All length or distance measurements were done using an image analysis software.

It must be mentioned that the after the experiments were completed, a simple test was done to verify the scaling technique used. In this test, the reference scale was placed both inside and outside the test chamber. Using both these readings to scale the length measurements showed that the difference between them was negligible (<0.5%).

Based on the measured bubble diameters, the rate of change of bubble diameter (dD_b/dt) was calculated. Knowing the position of the bubble normal to the heater surface and the liquid temperature profiles (measured separately), the liquid subcooling in the vicinity of the vapor bubble at each instant was determined. The condensation heat transfer coefficient, determined from the

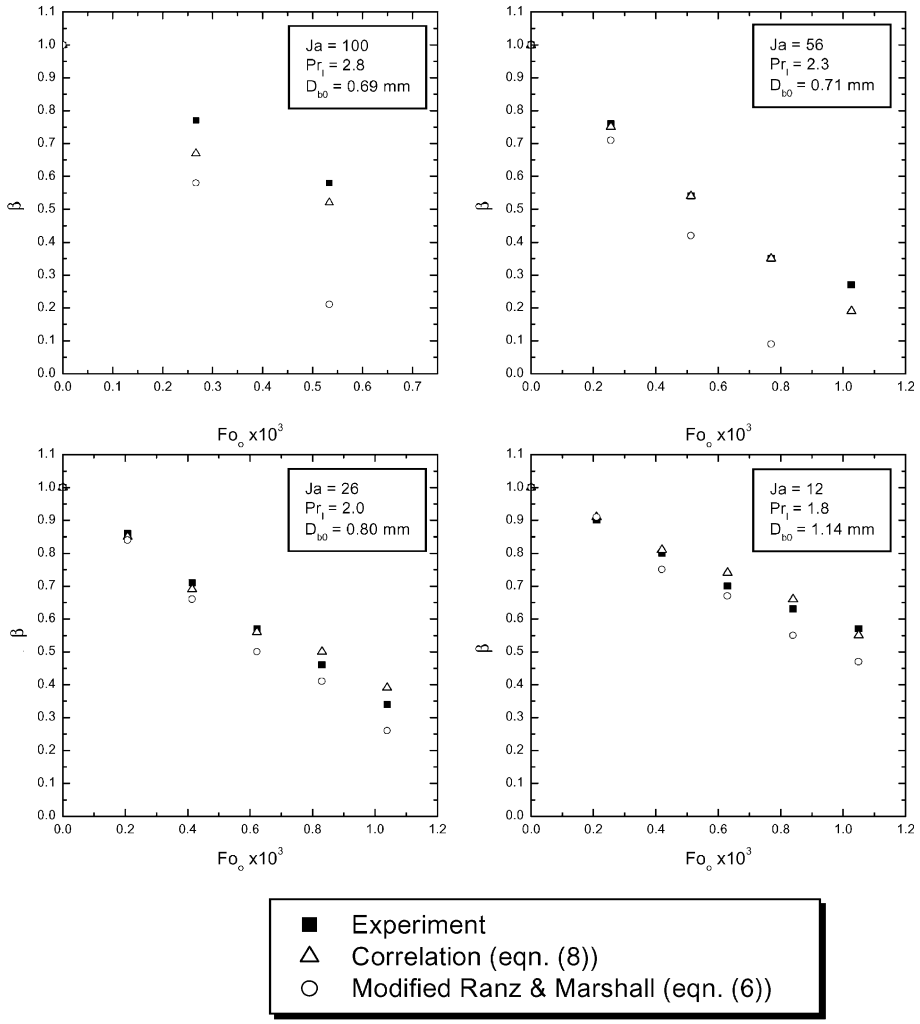

Fig. 7. Bubble diameter as a function of time.

energy balance around the collapsing bubble, can then be expressed as,

$$h_c = \frac{\rho_v h_{fg}}{2\Delta T_{sub}} \left(\frac{dD_b}{dt} \right) \quad (1)$$

where ΔT_{sub} is the instantaneous liquid subcooling. In calculating the instantaneous ΔT_{sub}, it must be mentioned that it is assumed that the measured liquid temperature profile (as shown in Fig. 5) is steady (i.e., does not change during the time it takes to record the movies) and that the bubble is translating in this known temperature field. Hence, the instantaneous ΔT_{sub} is calculated by knowing the instantaneous position (center) of the bubble and the given temperature field. However close to the heated wall, where the liquid temperature gradients are the largest, since the bubbles are in contact with hotter liquid on one side and colder liquid on the other, the local ΔT_{sub} (calculated as the mean of the two) could be different. From the data available in this study, it was estimated that the difference in the local ΔT_{sub} calculated using the two methods varied from 0.2% to 1.4%. However, since the bubbles typically move away quite rapidly from the heated wall, the overall effect of this variation is expected to be small. Once the local ΔT_{sub} was calculated, it was assumed to be uniform around the bubble.

Fig. 6 shows a sequence of nine photographs showing a bubble lifting off the heater surface and collapsing in the bulk liquid. The photographs are arranged in order from left to right and from top to bottom. The time interval between frames is 0.8 ms. Arrows shown in Fig. 6 point to the particular bubble of interest. The bubble diameters were measured until either the bubble moved out of the focusing area or moved out of the focusing plane of the camera or completely collapsed. The absolute bubble velocities were determined by calculating the change in bubble position (measured from high-speed movies) as a function of time. To account for the presence of the heating surface, the universal turbulent velocity profile (Kays and Crawford [7]) was used to determine the local liquid velocity. Though this velocity profile does not account for the two-phase flow, the impact of this expected to be minimal since most of the bubble is already outside the region where the velocity gradient is large (close to the wall), and also because the bubbles move away from the wall quite rapidly. Since the void fraction in most of the experiments were low (estimated from the video frames to be in the range 0.02–0.05) the presence of multiple bubbles is not expected to change the liquid velocity significantly. Once the condensation heat transfer rates and bubble velocities for individual bubbles were determined, an attempt was made to correlate the experimental data in terms of relevant dimensionless parameters. The following section describes the development of this new correlation.

The first step in developing this correlation was the assumption that the condensation Nusselt number (Nu_c) had the same functional dependence on the bubble Reynolds (Re_b) and Prandtl number (Pr_l) as suggested by the Ranz and Marshall [8] correlation (for forced convection around a solid sphere), i.e.,

$$Nu_c = \frac{h_c D_b}{k_l} = 0.6 Re_b^{1/2} Pr_l \quad (2)$$

It must be kept in mind that the above correlation (Eq. (2)) is for single phase forced convection around a solid sphere and that the minimum value of Nu_c in Eq. (2) is two. In Eq. (2), the bubble Reynolds number is defined as,

$$Re_b = \frac{\rho_l U_{b,rel} D_b}{\mu_l} \quad (3)$$

and

$$U_{b,rel} = \sqrt{(U_{b,z} - U_l)^2 + (U_{b,y})^2} \quad (4)$$

where $U_{b,z}$ and $U_{b,y}$ are the instantaneous absolute bubble velocities in the axial (z) and normal (y) directions, respectively. It was assumed that the bubbles had zero velocity in the x direction, since it could not be measured in the present set of experiments. However, due to the fact that in most experiments, the bubbles only appear to translate very little (from high-speed movies) in the transverse direction (x direction) as a result of the turbulent fluctuations in the flow, the velocity in the x direction is expected to be small.

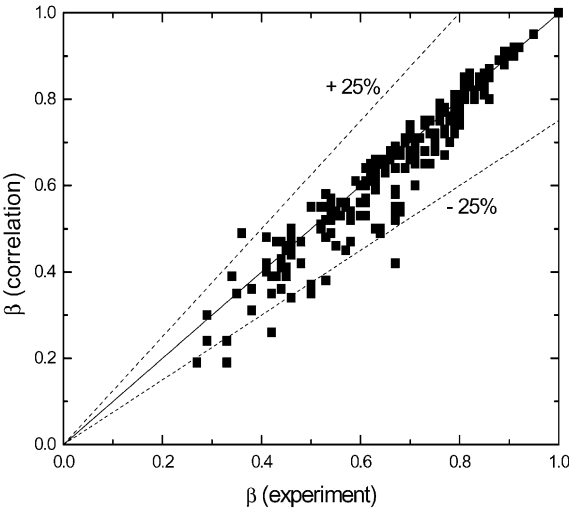

Fig. 8. Comparison of experimental data with predicted values of bubble collapse.

Substituting for h_c (from Eq. (2)) in Eq. (1) and rearranging yields, (5)

$$\frac{dD_b^{1/2}}{dt} = -1.2k_l\left(\frac{\rho_l U_{b,rel}}{\mu_l}\right)^{1/2} Pr_l^{1/3}\left[\frac{\Delta T_{sub}}{\rho_v h_{fg}}\right] \quad (5)$$

Integrating Eq. (5) with respect to time (t) and then nondimensionalizing yields the final expression for the dimensionless bubble diameter, β, as,

$$\beta^{3/2} = 1 - 1.8 Re_{bo}^{1/2} Pr_l^{1/3} Ja Fo_o \quad (6)$$

where Re_{bo} is the bubble Reynolds number based on D_{bo}. In Eq. (6), the Fourier number (Fo_o) is defined as,

$$Fo_o = \frac{\alpha t}{D_{bo}^2} \quad (7)$$

where α is the thermal diffusivity of the liquid ($\alpha = k_l/\rho_l C_{p,l}$). In Fig. 7, the dimensionless bubble diameters predicted using Eq. (6) are shown using open circles. From Fig. 7 it is clear that the modified Ranz and Marshall correlation underpredicts the measured values in all cases, especially at higher Ja values and at longer times (higher Fo_o values).

This under prediction is a result of the fact that as the bubble shrinks in size, the thermal layer around the bubble thickens. This behavior is not included in the correlations such as that due to Ranz and Marshall. The net effect of the thickening of the boundary layer is a

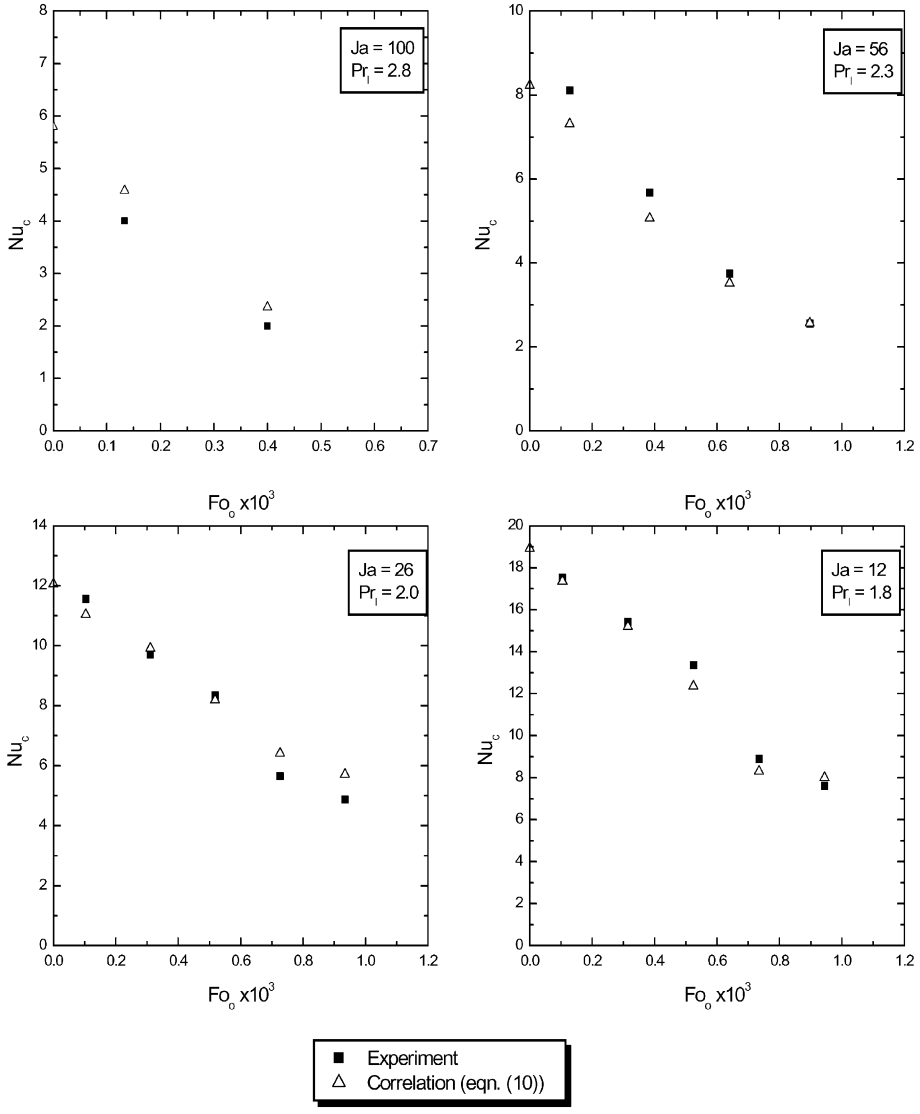

Fig. 9. Condensation Nusselt number variation with time.

decrease in the overall condensation rate. This situation can be visualized as being very similar to what happens when one has forced convection in the presence of blowing at the wall. This means that there are two separate time scales involved in this process, one due to forced convection heat transfer and the second due to the thickening of the thermal boundary layer. The thickening of the boundary layer not only depends on time but also on liquid subcooling.

To better predict β, a new correlation was developed by modifying Eq. (6) using a function of both Ja and Fo_o. The resulting correlation is given as,

$$\beta^{3/2} = 1 - 1.8 Re_{bo}^{1/2} Pr_l^{1/3} Ja\, Fo_o [1 - 0.72 Ja^{9/10} Fo_o^{2/3}] \quad (8)$$

The bubble diameters predicted using Eq. (8) are shown in Fig. 7 as open triangles. It can clearly be seen that the new correlation predicts the measured values very well. A comparison of all the measured data (total of 300 data points) and the corresponding predicted values (from Eq. (8)) are shown in Fig. 8. From Fig. 8 it can be seen that the new correlation (Eq. (8)) predicts most of the measured data to within ±25%.

Based on Eq. (8) a new correlation was also developed for Nu_c. Differentiating Eq. (8) with respect to time yields the following expression for dD_b/dt:

$$\frac{dD_b}{dt} = -1.2 \left[\frac{D_{bo}^{3/2}}{D_b^{1/2}}\right] Re_{bo}^{1/2} Pr_l^{1/3} Ja \left\{ \frac{\alpha_l}{D_{bo}^2} - 0.72 \left(\frac{5}{3}\right) Ja^{9/10} \left(\frac{\alpha_l}{D_{bo}^2}\right)^{5/3} t^{2/3} \right\} \quad (9)$$

Substituting Eq. (9) into Eq. (1), the final expression for Nu_c is given as,

$$Nu_c = \frac{h_c D_b}{k_l} = 0.6 Re_b^{1/2} Pr_l^{1/3} [1 - 1.20 Ja^{9/10} Fo_o^{2/3}] \quad (10)$$

Fig. 9 shows a comparison of the calculated Nu_c values and those predicted using Eq. (10), for the same cases as those in Fig. 7. The agreement between the calculated and predicted values is good. Since the condensation heat transfer rate was determined using the bubble diameters at two consecutive time steps (say t_1 and t_2), the calculated value of Nu_c is therefore applicable at a time step $(t_1 + t_2)/2$. Hence, referring to Fig. 9, it can be seen that the Nu_c data have been plotted for those Fo_o that correspond to the midpoint of two consecutive bubble diameters.

Analyzing the Nu_c correlation (Eq. (10)) in greater detail reveals the fact that the contribution due to forced convection heat transfer around the bubble is accounted for by the term $0.6 Re_b^{1/2} Pr_l^{1/3}$ (from the Ranz and Marshall correlation—which accounts for forced convection around a solid sphere), while the factor $(1 - 1.20\, Ja^{9/10} Fo_o^{2/3})$ is a correction term that accounts for the decrease in the condensation rate due to the thickening of the thermal boundary layer around the bubble. Additionally, since the correlations developed are based on a volume equivalent bubble diameter, these correlations do not differentiate between spherical and nonspherical bubbles. In the present set of experiments, the ratio of the major to minor diameters varied from 1.0 (for spherical bubbles) to 1.33 (for nonspherical bubbles).

Fig. 10 shows a comparison of all the calculated data (total of 300 data points) and the corresponding predicted values for Nu_c (from Eq. (10)). In most cases, the difference between the calculated and predicted values is within ±25%. The applicability of the new correlations for β (Eq. (8)) and Nu_c (Eq. (10)) are strictly limited to the following range of parameters: $20 < Re_b < 700$, $1.8 < Pr_l < 2.9$, and $12 < Ja < 100$. Also, it is important to keep in mind that the Eq. (10) is only valid when the predicted value of $Nu_c \geqslant 2$.

Fig. 11 shows a comparison of the proposed correlation (Eq. (8)) for the bubble diameter with some of the models reported in the literature. Though the models reported in the literature were developed based on experimental apparatus and techniques different from that used in this study, a direct comparison of the correlations developed is possible provided the local temperature field is accounted for properly. From Fig. 11, it is clear that Chen and Mayinger's [4] correlation underpredicts the bubble diameter at all Ja values ($Ja = 12$–100). On the other hand, Isenberg and Sideman's [3] correlation correctly predicts the bubble diameters at all Ja values ($Ja = 12$–100). Since Zeitoun et al. [5] correlation is in terms of the void fraction, two curves were plotted in Fig. 11—corresponding to the maximum

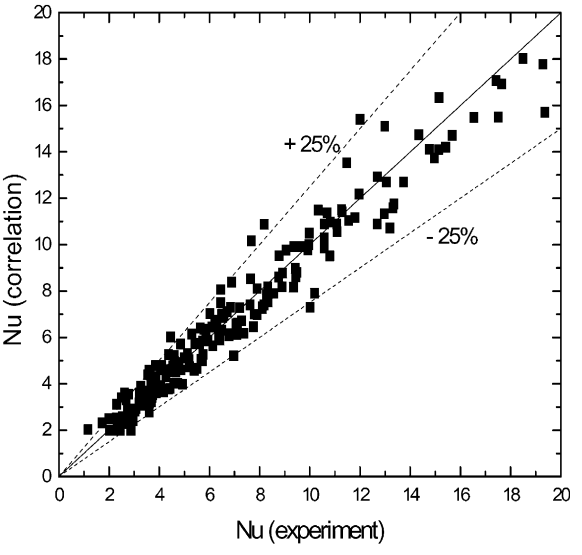

Fig. 10. Comparison of experimental data with predicted values of condensation Nusselt number.

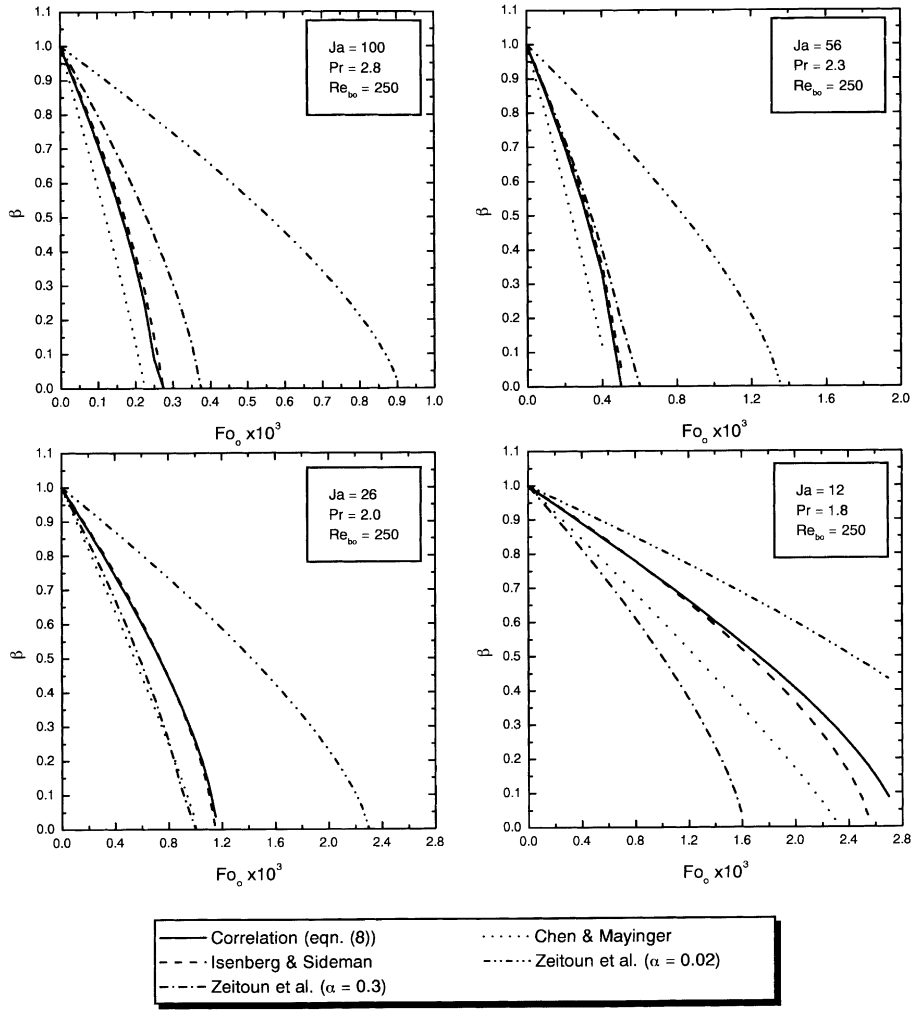

Fig. 11. Comparison of present correlation for bubble collapse with previous models.

($\alpha = 0.3$) and minimum ($\alpha = 0.02$) values of α. From Fig. 11, it can be seen that for $Ja < 56$, the predictions of the present correlation are bounded by those of Zeitoun et al. For, $Ja \geqslant 56$, Zeitoun et al.'s correlation always predict larger bubble diameters.

Fig. 12 shows a comparison of the proposed correlation for Nu_c with previous models for various Ja and Pr_l values. In comparing these models it is important to point out that in all of the previous models, the dependence of Nu_c on time is not explicit, rather it is implicitly included in Re_b ($Re_b = \beta Re_{bo}$, where β is a function of time). On the other hand, in the proposed correlation (Eq. (10)) the effect of time is included both implicitly and explicitly—implicitly through Re_b and explicitly through the factor $(1 - 1.20Ja^{9/10}Fo_o^{2/3})$. From Fig. 12, it is clear that the predictions of Isenberg and Sideman and Chen and Mayinger are in general agreement with the predictions from Eq. (10), though their correlations do not correctly account for the transient variation of the heat transfer coefficient even when all of the other parameters remain fixed. Since Zeitoun et al.'s correlation for Nu_c involves the mean Sauter diameter (D_{bs}) and because it is not clear what value of D_{bs} is to be chosen (D_{bs} is neither the initial nor the instantaneous bubble diameter), this correlation is not compared with the Nu_c correlation developed in this study.

It must be mentioned that a pure heat diffusion model was also considered in trying to estimate the heat transfer from the collapsing bubble (especially for low Re_b), but it was not successful. This model tended to predict a much higher condensation rate in the initial stages of bubble collapse because of the initial condition chosen (i.e., the bubble interface, initially at saturation temperature, is suddenly assumed to come in contact with the subcooled liquid). Additionally, the moving boundary model proposed by Riznic et al. [9] to account

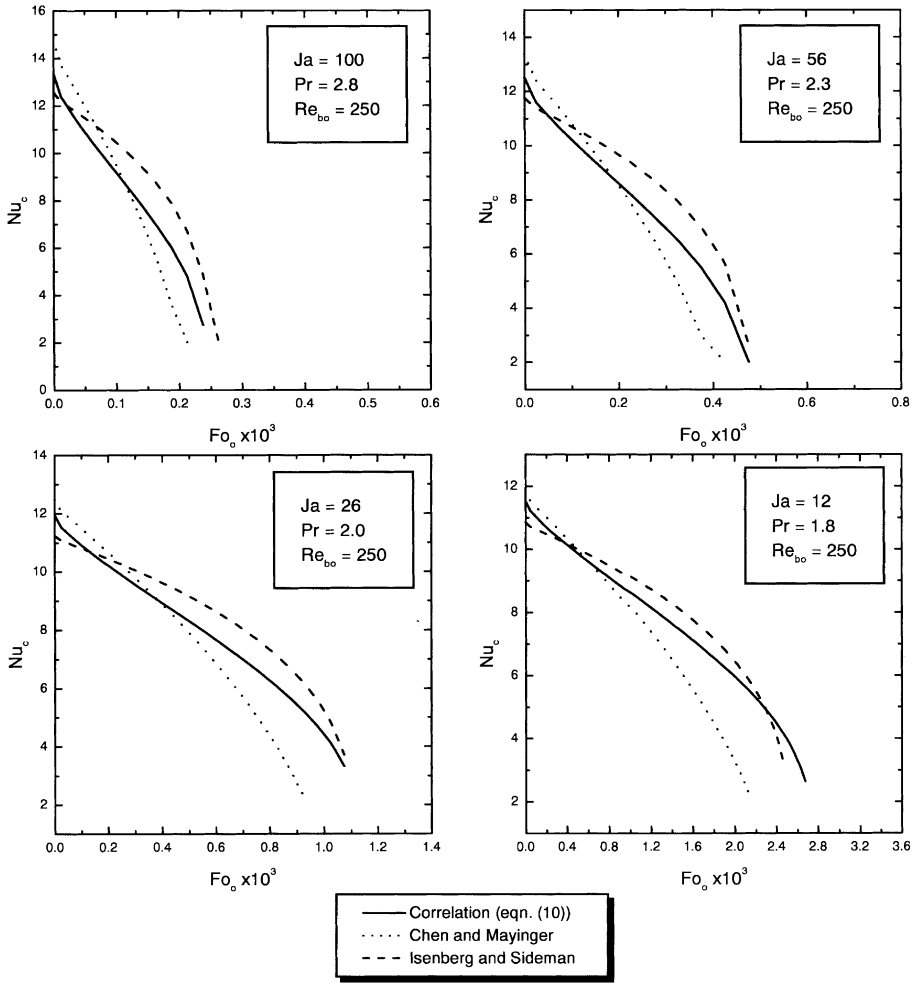

Fig. 12. Comparison of present correlation for condensation Nusselt number with previous models.

for the transient heat conduction from a growing or collapsing spherical vapor bubble in stagnant liquid was also considered. As in the previous model, this model too predicts a much larger Nu_c in the initial stages of bubble collapse. The main reason for this is the fact that the exact value of the thermal boundary layer thickness is not known apriori.

4. Summary and conclusion

Experimental data on bubble condensation during subcooled flow boiling was obtained. From the digitized images of collapsing bubbles and the local liquid subcooling, the bubble collapse rate and corresponding condensation heat transfer rate were determined. Based on the experimental data, two correlations have been proposed—one for the bubble collapse history and the other for the corresponding condensation Nusselt number. The correlations for these parameters are functions of the relevant dimensionless variables, namely Re_b, Pr_l, Ja, and Fo_o and for the first time correctly accounts for the effect of the forced convection heat transfer and thickening of the thermal boundary layer due to recession of the interface as condensation proceeds. These correlations have been compared with some of the correlations available in the literature. The correlations cover the following range of parameters: $20 < Re_b < 700$, $1.8 < Pr_l < 2.9$, and $12 < Ja < 100$. The present correlations were developed for low void fractions.

Though the correlation developed for Nu_c depends on D_b and D_{bo}, we believe that this is the correct approach if one were to develop a mechanistic model for the process, since it correctly capture the physics involved. Modification of the correlation to better suit the requirements

of two-fluid modeling codes (e.g., RELAP5) can be easily made. When using the correlations developed in this study as a closure equation in a two-fluid model, it is assumed that information regarding the initial bubble diameter (D_{bo}) is already available (from experimental data or correlations).

Acknowledgements

This work received support from the United States Nuclear Regulatory Commission.

References

[1] RELAP5/MOD3 Code Manual, vol. 1, Code Structure, System Models, and Solution Methods, INEL-95/0174, NUREG/CR-5535, August 1995.

[2] G.R. Warrier, V.K. Dhir, Review of experimental and analytical studies on low pressure subcooled flow boiling, in: Proceedings of the Fifth ASME/JSME Joint Thermal Engineering Conference, Paper AJTE99-6233, 1999, CD-ROM Edition.

[3] J. Isenberg, S. Sideman, Direct contact heat transfer with change of phase: bubble condensation in immiscible liquids, Int. J. Heat Mass Transfer 13 (1970) 997–1011.

[4] Y.M. Chen, F. Mayinger, Measurement of heat transfer at phase interface of condensing bubbles, Int. J. Multiphase Flow 18 (1992) 877–890.

[5] O. Zeitoun, M. Shoukri, V. Chatoorgoon, Interfacial heat transfer between steam bubbles and subcooled water in vertical upward flow, ASME J. Heat Transfer 117 (1995) 402–407.

[6] G.R. Warrier, N. Basu, V.K. Dhir, Subcooled boiling at low pressures, Annual Progress Report for USNRC Task Order 5, Report No. UCLA ENG-99-211, 1999.

[7] W.M. Kays, M.E. Crawford, Convective Heat and Mass Transfer, third ed., McGraw-Hill, New York, 1993.

[8] E. Ranz, W.R. Marshall, Evaporation from droplets: parts I and II, Chem. Eng. Prog. 48 (1952) 141–146, 173–180.

[9] J. Riznic, G. Kojasoy, N. Zuber, On the spherically symmetric phase change problem, Int. J. Fluid Mech. Res. 26 (2) (1999) 136–171.